Dalton Transactions

ROYAL SOCIETY OF CHEMISTRY

COMMUNICATION

View Article Online
View Journal | View Issue

Open Access Article. Published on 01 2024. Downloaded on 2024/8/14 22:05:45.
This article is licensed under a Creative Commons Attribution 3.0 Unported Licence.

Check for updates

Cite this: *Dalton Trans.*, 2024, **53**, 8541

Received 30th April 2024,
Accepted 1st May 2024

DOI: 10.1039/d4dt01273a

rsc.li/dalton

Monitoring structure and coordination chemistry of Co_4O_4-based oxygen evolution catalysts by nitrogen-14/-15 and cobalt-59 NMR spectroscopy†‡

Felix Uhlig,§[a] Michael B. Stammler,¶[a] Florian Meurer,[a,b] Ilya G. Shenderovich,[c] Jan Blahut *[d] and Florian M. Wisser *[a,e]

The structural features of cobalt-based oxygen evolution catalysts are elucidated by combining high-field MAS NMR spectroscopy and DFT calculations. The superior photocatalytic activity of the heterogeneous system over its homogeneous counterpart is rationalised by the structural features. The higher activity is caused by a more favourable electron-withdrawing character of the framework.

Transition metal (TM) cubanes are a class of organometallic compounds that contain an M_4O_4 cube as a core, typically surrounded by nitrogen and oxygen donor ligands.[1–3] Most complexes have pyridine- or bipyridine-based axial ligands while the equatorial facets of the cube are bridged by carboxylates. TM cubanes have been studied extensively in the last decade mainly for three reasons. First, their structure is similar to the active site in photo system II (PS II), which consists of a $\{CaMn_4O_5\}$ oxo cluster, making them ideal model systems to study the oxygen evolution reaction (OER). Second, the large number of TM and TM combinations opens up the possibility to vary the metal core by design. Third, the rich coordination chemistry of TM allows the design of an almost infinite number of cubanes by exchanging axial pyridines and/or equatorial carboxylates.[1,3] Although cubanes have been widely studied as OER catalysts or in selective oxidation reactions, surprisingly their characterisation by (solid-state) nuclear magnetic resonance spectroscopy remains scarce, except for the standard ^{1}H and ^{13}C liquid NMR characterisation. As with other metal–organic complexes, ^{15}N NMR and NMR studies of the metal are expected to provide important insights into the local structure.[4,5] To this end tetrakis[(μ-acetato-κO′κO′)-μ3-oxo-(pyridine)cobalt(III)][6] ($Co_4O_4(OAc)_4Py_4$, Fig. 1) is an ideal model, not only because of its high catalytic activity, but also because the central Co is NMR active (100% natural abundance) with the largest chemical shift range.[7] Furthermore, ^{59}Co is a quadrupolar nucleus with a spin of 7/2, so the linewidth of the ^{59}Co NMR signal is therefore highly sensitive to the symmetry of the ligand atom combination.

Here we showcase the detailed insight into the local structure of $Co_4O_4(OAc)_4Py_4$ available from both liquid- and solid-state NMR spectroscopy. In addition to $Co_4O_4(OAc)_4Py_4$, we also studied its ^{15}N-labelled analogue $Co_4O_4(OAc)_4\{^{15}N\}Py_4$ and a $Co_4O_4(OAc)_4Py_4$ derived porous coordination polymer (PCP).[8] Solid-state ^{15}N NMR spectroscopic studies, either under magic angle spinning (MAS) or static, provide additional information not accessible from liquid-state NMR spectroscopy. By combining ^{15}N NMR with DFT calculations, we highlight the effect of Co coordination on the chemical shift tensors of ^{15}N and on the resulting isotropic chemical shift. In addition, liquid-state ^{15}N and ^{59}Co NMR spectroscopy reveal the stable coordination of axial pyridine ligands, the (partial) exchange of equatorial acetate ligands, and the intact structure of the Co_4O_4 core, even after photocatalysis. In order to obtain useful nitrogen-15 NMR spectra in a reasonable time, labelling schemes are essential.[9] While this is feasible for molecular complexes with simple ligands such as pyridine, solid materials require more complex ligands whose labelling leads to multi-step synthesis schemes. Although the natural abundance of ^{14}N is >99.6%, ^{14}N NMR spectroscopy remains

[a]University of Regensburg, Institute of Inorganic Chemistry, Universitätsstraße 31, 93053 Regensburg, Germany. E-mail: florian.wisser@fau.de
[b]Rossendorf Beamline, Helmholtz-Zentrum Dresden-Rossendorf, Dresden, Germany
[c]University of Regensburg, Institute of Organic Chemistry, Universitätsstraße 31, 93040 Regensburg, Germany
[d]Institute of Organic Chemistry and Biochemistry of the Czech Academy of Sciences, Flemingovo nám. 2, 166 10, Prague 6, Czech Republic. E-mail: jan.blahut@uochb.cas.cz
[e]Erlangen Center for Interface Research and Catalysis, Friedrich-Alexander-Universität Erlangen-Nürnberg, Egerlandstraße 3, 91058 Erlangen, Germany

† Raw data available on Zenodo: https://doi.org/10.5281/zenodo.10683598.

‡ Electronic supplementary information (ESI) available: Synthesis, additional characterization, catalysis and DFT calculations. CCDC 2239008. For ESI and crystallographic data in CIF or other electronic format see DOI: https://doi.org/10.1039/d4dt01273a

§ Present address: Bavarian Polymer Institute and Department of Chemistry, University of Bayreuth, Bayreuth 95447, Germany.

¶ Present address: University of Augsburg, Institute of Physics, Chair of Solid State and Materials Chemistry, Universitätsstraße 1, 86159 Augsburg, Germany.

Open Access Article. Published on 01 2024. Downloaded on 2024/8/14 22:05:45.
This article is licensed under a Creative Commons Attribution 3.0 Unported Licence.

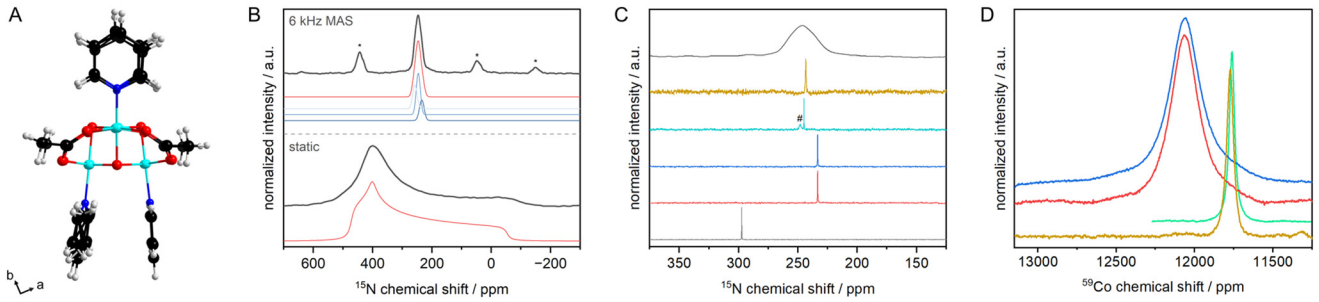

Fig. 1 (A) Molecular structure of $Co_4O_4(OAc)_4Py_4$ along the crystallographic *c* direction. Colour code: C: black, O: red, N: blue, Co: cyan and H white. (B) Solid state NMR spectra of $Co_4O_4(OAc)_4\{^{15}N\}Py_4$ with and without MAS as well as a deconvoluted spectra. (C) Comparison of ^{15}N NMR spectra of $Co_4O_4(OAc)_4\{^{15}N\}Py_4$ dissolved in D_2O (red), D_2O (pH > 9, blue), ACN-d3 (cyan), CD_2Cl_2 (orange) with the CP MAS spectrum (black) as well as the spectrum of pyridine in D_2O. # labels ^{15}N signal from ACN-d3. (D) Comparison of ^{59}Co NMR spectra of $Co_4O_4(OAc)_4\{^{15}N\}Py_4$ dissolved in D_2O (red), D_2O (pH > 9, blue), ACN-d3 (cyan) and CD_2Cl_2 (orange).

scarce.[10] Therefore, we have finally extended the investigation to the 3D solid material using proton-detected nitrogen-14 NMR spectroscopy at fast MAS and high field,[11,12] adding another proton-detected technique to the toolbox for PCP characterisation.[13]

The ^{15}N chemical shift of pyridine is very sensitive to the coordination or protonation of the N atom.[5] It is therefore an ideal descriptor to monitor changes in *e.g.* the structure of a pyridine-based complex. The solid state ^{15}N NMR spectrum of $Co_4O_4(OAc)_4\{^{15}N\}Py_4$ measured under static conditions shows a typical powder pattern from which the ^{15}N chemical shift tensor and the symmetry of the tensor have been extracted to be $\delta_t = 465$ (5) ppm (δ_{11}), $\delta_r = 405(5)$ ppm (δ_{22}) and $\delta_\perp = -54(1)$ ppm (δ_{33}, $\delta_{ref}(^{15}NH_3$ liq.) = 0 ppm). To obtain a deeper insight, DFT calculations of the chemical shifts were performed using the Polarisable Continuum Model approximation assuming that the effects of non-covalent interactions and the crystal field on the chemical shielding are small, and that a change in the dielectric constant has a negligible effect (see ESI‡ for details).[14,15] The calculated tensors vary between 480 ppm (δ_t), 440 ppm (δ_r) and −91 ppm ($\delta_\perp$), in good agreement with the observed values.

The solid-state ^{15}N NMR spectrum of $Co_4O_4(OAc)_4\{^{15}N\}Py_4$ recorded under MAS conditions, gives an isotropic chemical shift of 246.6 ppm, with a linewidth of 730 Hz. This rather large linewidth is most likely caused by the distribution of the N···Co distances, between 1.954(3) and 1.965(2) Å (Table S13‡).‖ At first sight, it can be assumed that there are three overlapping signals (239(3), 248(2), 259(2) ppm, Fig. 1b), with the central signal being twice as intense as the side ones. Indeed, we would expect such a pattern from the single crystal structure, as we see three sets of N···Co distances (Tables S5 and S7‡).

The effect of Co coordination on the ^{15}N chemical shift of pyridine is very different from that caused by hydrogen bonding. Hydrogen bonding leads to a strong change in the tangential component of the tensor.[16,17] Coordination to Co^{III}, however, leads to changes in both the tangential and the perpendicular components of the tensor (Tables S5 and S7‡). These changes are unidirectional and result in a large change in the isotropic value, compared to the chemical shift of free pyridine in the solid state (314 ppm (ref. 18)). Also compared to the impact of hydrogen bonding in the solid state, the change upon coordination in chemical shift ($\Delta\delta^{15}N$) of pyridine is large, with −68 ppm compared to −20 ppm in case of hydrogen bonding to water.[18] The $\Delta\delta^{15}N$ values observed both in the solid state and in solution (*vide infra*) for pyridine coordinated to Co^{III} in the cubane are in line with the reported $\Delta\delta^{15}N$ value for transition metal complexes containing pyridine-moieties as ligands.[5]

Next, we studied the cubane dissolved in different solvents. In aprotic solvents *i.e.* acetonitrile (244.8 ppm) and dichloromethane (243.3 ppm), the ^{15}N chemical shifts are in excellent agreement with the isotropic chemical shift observed by MAS NMR (246.6 ppm, Fig. 1c). When dissolved in neutral water or basic media (pH of catalysis, see below), the signal shifts to 233.3 ppm independent of the pH value. Thus, the N atom is more shielded in aqueous environments compared to the solid state or dissolved in aprotic solvents. Importantly, no traces of free or hydrogen-bonded pyridine are observed.[18] Thus, the small changes in chemical shift observed between aqueous and aprotic conditions as well as the solid state cannot be explained by de-coordination of a pyridine even in a very fast equilibrium. In the case of a fast equilibrium, a low field shift would have been expected, as only the time average of the chemical shifts would have been observed.[18] An increase in the Co···N bond length should result in a reduction of $\Delta\delta^{15}N$ (Tables S5 and S7‡) and thus in a low field shift of the isotopic chemical shift, which we did not observe. Although, the isotropic ^{15}N chemical shifts of the cubane are different in aqueous solution and in the polycrystalline state, the structure of the complex is preserved, *i.e.* the Co···N bond not only does not break in aqueous solutions but, apparently, becomes somewhat shorter.

We further studied the catalytically active Co_4O_4 core by ^{59}Co NMR spectroscopy. The linewidth of the ^{59}Co NMR signal is highly sensitive to the symmetry of the ligand atom combination.[19] With decreasing symmetry of the ligand atom combination, the NMR signal becomes broader or vanishes comple-

Open Access Article. Published on 01 2024. Downloaded on 2024/8/14 22:05:45.
This article is licensed under a Creative Commons Attribution 3.0 Unported Licence.

tely. The linewidth of the ^{59}Co chemical shift increases from 3.7 kHz in acetonitrile, 4.4 kHz in dichloromethane to more than 22.5 kHz in aqueous solution, again independent of the pH value (Fig. 1d). Similarly, for a series of Co complexes, a change in linewidth by a factor of approx. 6 has been reported when acetonitrile was replaced by water, the increase in linewidth has been attributed to additional hydrogen bonding interactions.[20] To allow for significant hydrogen bonding interaction with water, some of the labile acetate ligands are (partially) replaced by a water molecule and a hydroxyl group.[8] This ligand exchange not only allows for a better hydrogen bonding interaction, but also decreases the ligand group symmetry which may also contribute to the observed increase in linewidth.[21] Other effects that may affect the linewidth such as scalar coupling can be neglected as the ^{59}Co NMR spectra for complexes with ^{15}N-labelled and natural abundance pyridine gave the same linewidth (Fig. S1, and section S4‡ for further discussion). The chemical shift is also affected by the solvent and thus partial ligand exchange: from about 11 770 ppm for the pristine $Co_4O_4(OAc)_4Py_4$ to 12 070 ppm for the cubane in aqueous solution. Similarly, ^{59}Co NMR spectra can be acquired under MAS conditions (with spinning speed exceeding the second order quadrupolar shift). By recording spectra at two different magnetic fields, an isotropic ^{59}Co shift of 12 030 ppm was extracted for $Co_4O_4(OAc)_4Py_4$ in the solid state. Partial exchange of acetate by H_2O/OH is further evidenced by ^{1}H and ^{1}H–^{13}C double-CP MAS NMR spectra showing a signal at approx. −1 ppm, characteristic for isolated OH groups such as in MgO, γ-Al_2O_3 or zinc-based metal–organic frameworks.[22–24]

Advantageously, the NMR experiments discussed offer sufficient sensitivity to study $Co_4O_4(OAc)_4Py_4$ under catalytic conditions. In order to verify the catalytic activity, $Co_4O_4(OAc)_4Py_4$ was dissolved in an aqueous borate buffer at pH 8 containing 6 mM $Na_2S_2O_8$ as a sacrificial electron acceptor and 1 mM $Ru(bpy)_3Cl_2$ as photosensitiser. Irradiation with a 100 W lamp yields turnover frequencies of up to 1.3×10^{-3} s^{-1} (Fig. S3‡), in line with reports from Dismukes and co-workers (10^{-2} s^{-1}, pH 7, carbonate buffer, 250 W lamp)[25] or Sartorel and co-workers (0.2×10^{-3} s^{-1}, pH 8, borate buffer, 450 nm LEDs, Table S9‡).[26] To shed light on the molecular structure of the cubane after catalysis, the photocatalytic experiments were also performed in an NMR tube and in deuterated solvents under otherwise similar conditions. The ^{15}N NMR and ^{59}Co NMR spectra of the cubane dissolved in the reaction mixture and recorded before and after the reaction are the same as those observed in aqueous solutions (Fig. S4‡). No change in the ^{59}Co NMR linewidth is observed, confirming that no change in the molecular structure has occurred. Thus, a coordination of borate to the cubane core can be ruled out, which has been discussed in stabilizing the cubane core.[27] However, such a coordination would change the coordination sphere of the Co centre, affecting its linewidth (see above). Similarly, ^{1}H NMR spectra did not show any changes in the cubane signals, in particular no free pyridine is observed, nor are there any changes in the acetate region of the spectrum, in contrast to bipyridine-based analogues.[27]

To showcase the potential of NMR in establishing the local structure, *e.g.* Co's ligand group symmetry and N coordination, we also studied an amorphous PCP in which the cubane core acts as a node. In this PCP, the cubane nodes are interconnected with each other by replacing monodentate pyridine with tridentate 2,4,6-tri(4-pyridyl)-1,3,5-triazine (TPT) to form Co_4TPT (Fig. 2a).[8] First we demonstrate the activity of Co_4TPT as an OER photocatalyst in the presence of $Ru(bpy)_3Cl_2$ as a photosensitiser. Under otherwise identical conditions to $Co_4O_4(OAc)_4Py_4$, Co_4TPT gives a TOF of 3.0×10^{-3} s^{-1}, which is stable over several cycles (Fig. S5‡). Compared to the molecular $Co_4O_4(OAc)_4Py_4$, the TOF increases by a factor of 3 when using

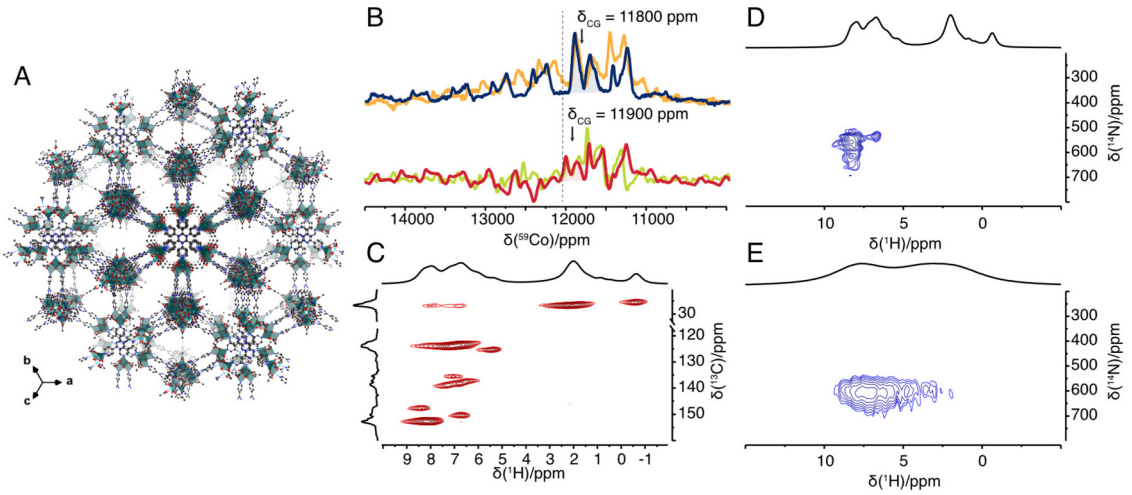

Fig. 2 (A) Idealised structural model of Co_4TPT.[8] (B) ^{59}Co solid-state NMR spectrum of $Co_4O_4(OAc)_4Py_4$ acquired under 70 kHz (blue), 62.5 kHz (orange) MAS rate at 14.09 T B_0 field (600 MHz) and under 55 kHz (red), 50 kHz (green) MAS rate at 18.79 T B_0 field (800 MHz) with indicated centre of gravity of the isotropic signal and pure isotropic chemical shift of 12 030 ppm (dashed line). (C) 2D ^{1}H–^{13}C double-CP spectrum of $Co_4O_4(OAc)_4Py_4$. (D and E) 2D ^{1}H–^{14}N TRAPDOR-HMQC spectrum of $Co_4O_4(OAc)_4Py_4$ (D) and of Co_4TPT (E). All spectra in (C–E) were recorded at a MAS frequency of 62.5 kHz MAS rate at 14.09T.

Open Access Article. Published on 01 2024. Downloaded on 2024/8/14 22:05:45.
This article is licensed under a Creative Commons Attribution 3.0 Unported Licence.

the heterogeneous catalyst (Fig. S3‡). The higher activity of Co_4TPT is not due to decomposition of the cubane core after heterogenization. First, only traces of leached Co species are detected in the supernatant after each cycle (Table S10‡). Note that traces of decomposed cubane, the presence of which depends on the reaction conditions, have been reported to be catalytically inactive.[26] Second, the IR spectrum of the spent catalyst confirms the stable nature of the framework, *i.e.* the Co···TPT coordination bonds, with the labile acetate ligands most likely replaced by water and OH groups (Fig. S6 & ESI‡ for further discussion).[8,28] Finally, the presence of free pyridine moieties,[8] which could be responsible for the change in activity, was ruled out by ^{14}N solid-state NMR spectroscopy (see below). Thus, the higher activity of Co_4TPT compared $Co_4O_4(OAc)_4Py_4$ is most likely due to the change of the electron density on the active cubane core. The replacement of a proton (Hammett constant of 0) in the 4-position of the pyridine by a triazine core (Hammett constant of 0.29[29]) in the framework TPT-linker causes a lower electron density on the pyridine and subsequently on the Co core. For a series of molecular cubanes, Wang *et al.* correlated a lower electron density on the Co core with a higher reaction rate.[30] The PCP framework controls the catalytic activity in the same way as a molecular ligand in homogeneous catalysis and thus behaves as a macroligand in oxidative reactions. Similar behaviour of different PCPs has already been demonstrated for various reduction reactions.[31–33]

To rule out that free pyridine moieties[8] are responsible for the change in activity, we studied Co_4TPT by solid-state NMR spectroscopy. Selective labelling of the linker TPT with ^{15}N on its pyridyl moiety would require multi-step synthesis schemes. To avoid such costly schemes, we have instead studied the amorphous PCP using proton-detected nitrogen-14 NMR spectroscopy (TRAPDOR-HMQC).[12] For comparison, the molecular cubane was also studied using the same techniques. In contrast to the molecular complex, the ^{1}H NMR spectrum of the amorphous PCP shows two broad peaks at around 7 and 3 ppm of aromatic and aliphatic protons, respectively. Likewise, the ^{13}C NMR spectrum shows broader peaks and thus loses some of the fine information obtained for the molecular complex (Fig. S2‡). However, the proton-detected ^{14}N NMR experiments yield very similar ^{14}N chemical shifts for the pyridine moiety centred at around 600 ppm (Fig. 2D and E). This confirms the very similar coordination geometry of the pyridine N atoms in $Co_4O_4(OAc)_4Py_4$ and Co_4TPT. In addition, observed difference between ^{15}N and ^{14}N shift allows estimation of ^{14}N quadrupolar coupling constant to C_Q = 2.9 MHz (assuming η = 0 see ESI 5.3‡). Note that similar differences between the observed nitrogen-14 and nitrogen-15 shifts have previously been described and are caused by the contribution of the isotropic second order quadrupolar shift to the nitrogen-14 shift.[12,34] All together with the knowledge obtained from pair distribution function analysis and X-ray absorption spectroscopy that the Co_4O_4 core remains intact after integration into the amorphous PCP,[8] we now have a complete picture of the molecular structure of the active site.

Conclusions

We have demonstrated a step forward in the analysis of Co_4O_4-based model catalyst of nature's PS II, made possible by combining $^{14/15}$N and ^{59}Co liquid-state NMR with solid-state NMR under high MAS rates and carefully tuned pulse sequences, and DFT calculations. This allows to understand changes in N···Co coordination distance on ^{15}N chemical shift, to assign all nitrogen resonances resolved in the spectrum of the molecular complex $Co_4O_4(OAc)_4Py_4$ and to disclose its behaviour under catalytic conditions. For the first time the coordination chemistry of pyridine moieties in an amorphous PCP has been determined, which is crucial for the understanding of their catalytic performance. The reported proton-detected ^{14}N NMR experiments are an important addition to the conventional repertoire of solid-state NMR. Notably, they allow to avoid costly and challenging labelling schemes to introduce ^{15}N atoms at selected positions on the molecules, and allow a reduction in the amount of sample required, which in turn allows to use of fast MAS to achieve high spectral resolution, thus increasing the amount of information.

Author contributions

F.U.: investigation (synthesis, catalysis), writing – review. M.S.: investigation (synthesis, characterization), writing – review. F.M.: investigation (SC XRD), formal analysis, writing – review. I.G.S.: investigation (solid state NMR & calculations), writing – original draft, review & editing. J.B. investigation (solid state NMR), conception, writing – original draft, review & editing. F.M.W.: formal analysis, conception, writing – original draft, review & editing, supervision.

Conflicts of interest

There are no conflicts to declare.

Acknowledgements

J. B. acknowledge Prof. Eike Brunner (TU Dresden) for experimental time for high-field ^{59}Co and Czech Science Foundation (24-10843S) for financial support. F. M. is grateful to the Studienstiftung des Deutschen Volkes for a PhD fellowship.

References

‖Crystallographic data for $Co_4O_4(OAc)_4Py_4$ are provided as cif file (CCDC 2239008‡).

1 J. Li, C. A. Triana, W. Wan, D. P. Adiyeri Saseendran, Y. Zhao, S. E. Balaghi, S. Heidari and G. R. Patzke, *Chem. Soc. Rev.*, 2021, **50**, 2444–2485.

 This journal is © The Royal Society of Chemistry 2024

Open Access Article. Published on 01 2024. Downloaded on 2024/8/14 22:05:45.
This article is licensed under a Creative Commons Attribution 3.0 Unported Licence.

2 J. Amtawong, A. I. Nguyen and T. D. Tilley, *J. Am. Chem. Soc.*, 2022, **144**, 1475–1492.
3 Y. Zhao, D. P. Adiyeri Saseendran, C. Huang, C. A. Triana, W. R. Marks, H. Chen, H. Zhao and G. R. Patzke, *Chem. Rev.*, 2023, **123**, 6257–6358.
4 R. W. Schurko and R. E. Wasylishen, *J. Phys. Chem. A*, 2000, **104**, 3410–3420.
5 L. Pazderski, in *Annual Reports on NMR Spectroscopy*, Elsevier Ltd, 1st edn, 2020, vol. 101, pp. 151–284.
6 R. Chakrabarty, S. J. Bora and B. K. Das, *Inorg. Chem.*, 2007, **46**, 9450–9462.
7 P. Granger, in *Encyclopedia of Magnetic Resonance*, John Wiley & Sons, Ltd, Chichester, UK, 2007.
8 A. I. Nguyen, K. M. Van Allsburg, M. W. Terban, M. Bajdich, J. Oktawiec, J. Amtawong, M. S. Ziegler, J. P. Dombrowski, K. V. Lakshmi, W. S. Drisdell, J. Yano, S. J. L. Billinge and T. D. Tilley, *Proc. Natl. Acad. Sci. U. S. A.*, 2019, **116**, 201815013.
9 R. Jabbour, C. W. Ashling, T. C. Robinson, A. H. Khan, D. Wisser, P. Berruyer, A. C. Ghosh, A. Ranscht, D. A. Keen, E. Brunner, J. Canivet, T. D. Bennett, C. Mellot-Draznieks, A. Lesage and F. M. Wisser, *Angew. Chem., Int. Ed.*, 2023, **62**, e202310878.
10 H.-L. Deng, X.-S. Luo, Z. Lin, J. Niu and M.-H. Huang, *J. Org. Chem.*, 2021, **86**, 16699–16706.
11 Y. Nishiyama and N. T. Duong, *J. Magn. Reson. Open*, 2022, **10–11**, 100062.
12 B. P. Tatman, H. Modha and S. P. Brown, *J. Magn. Reson.*, 2023, **352**, 107459.
13 J. Blahut, A. L. Lejeune, S. Ehrling, I. Senkovska, S. Kaskel, F. M. Wisser and G. Pintacuda, *Angew. Chem., Int. Ed.*, 2021, **60**, 21778–21783.
14 I. G. Shenderovich, *J. Phys. Chem. A*, 2023, **127**, 5547–5555.
15 I. G. Shenderovich and G. S. Denisov, *Molecules*, 2021, **26**, 1283.
16 M. S. Solum, K. L. Altmann, M. Strohmeier, D. A. Berges, Y. Zhang, J. C. Facelli, R. J. Pugmire and D. M. Grant, *J. Am. Chem. Soc.*, 1997, **119**, 9804–9809.
17 P. Lorente, I. G. Shenderovich, N. S. Golubev, G. S. Denisov, G. Buntkowsky and H.-H. Limbach, *Magn. Reson. Chem.*, 2001, **39**, S18–S29.
18 S. Sharif, I. G. Shenderovich, L. González, G. S. Denisov, D. N. Silverman and H.-H. Limbach, *J. Phys. Chem. A*, 2007, **111**, 6084–6093.
19 N. Juranić, *Coord. Chem. Rev.*, 1989, **96**, 253–290.
20 S. C. F. Au-Yeung and D. R. Eaton, *J. Magn. Reson.*, 1983, **52**, 366–373.
21 A. Yamasaki, *J. Coord. Chem.*, 1991, **24**, 211–260.
22 C. Chizallet, H. Petitjean, G. Costentin, H. Lauron-Pernot, J. Maquet, C. Bonhomme and M. Che, *J. Catal.*, 2009, **268**, 175–179.
23 A. T. F. Batista, D. Wisser, T. Pigeon, D. Gajan, F. Diehl, M. Rivallan, L. Catita, A.-S. Gay, A. Lesage, C. Chizallet and P. Raybaud, *J. Catal.*, 2019, **378**, 140–143.
24 S. Glante, D. Wisser, M. Hartmann, M. Joos, R. E. Dinnebier and S. Bette, *Cryst. Growth Des.*, 2022, **22**, 3795–3807.
25 N. S. McCool, D. M. Robinson, J. E. Sheats and G. C. Dismukes, *J. Am. Chem. Soc.*, 2011, **133**, 11446–11449.
26 A. Genoni, G. La Ganga, A. Volpe, F. Puntoriero, M. Di Valentin, M. Bonchio, M. Natali and A. Sartorel, *Faraday Discuss.*, 2015, **185**, 121–141.
27 P. F. Smith, C. Kaplan, J. E. Sheats, D. M. Robinson, N. S. McCool, N. Mezle and G. C. Dismukes, *Inorg. Chem.*, 2014, **53**, 2113–2121.
28 A. I. Nguyen, J. Wang, D. S. Levine, M. S. Ziegler and T. D. Tilley, *Chem. Sci.*, 2017, **8**, 4274–4284.
29 M. A. Fávaro, J. Yang, D. Ditz, H. Küçükkeçeci, M. H. Alkhurisi, S. Bergwinkl, A. Thomas, E. A. Quadrelli, R. Palkovits, J. Canivet and F. M. Wisser, *ChemCatChem*, 2023, **15**, e202300197.
30 Z. Luo, Y. Hou, J. Zhang, S. Wang and X. Wang, *Beilstein J. Org. Chem.*, 2018, **14**, 2331–2339.
31 F. M. Wisser, P. Berruyer, L. Cardenas, Y. Mohr, E. A. Quadrelli, A. Lesage, D. Farrusseng and J. Canivet, *ACS Catal.*, 2018, **8**, 1653–1661.
32 F. M. Wisser, Y. Mohr, E. A. Quadrelli, D. Farrusseng and J. Canivet, *ChemCatChem*, 2018, **10**, 1778–1782.
33 F. M. Wisser, Y. Mohr, E. A. Quadrelli and J. Canivet, *ChemCatChem*, 2020, **12**, 1270–1275.
34 A. S. Tatton, T. N. Pham, F. G. Vogt, D. Iuga, A. J. Edwards and S. P. Brown, *CrystEngComm*, 2012, **14**, 2654–2659.